

Occurrence of Excess ^{40}Ar in Amphibole: Implications of $^{40}\text{Ar}/^{39}\text{Ar}$ Dating by Laser Stepwise Heating and *in vacuo* Crushing



Rong-Guo Hu^{1,2}, Xiu-Juan Bai³, Jan Wijbrans², Fraukje Brouwer², Yi-Lai Zhao¹, Hua-Ning Qiu^{3,4}

1. College of Earth Sciences, Guangxi Key Laboratory of Hidden Metallic Ore Deposits Exploration, Guilin University of Technology, Guilin 541004, China

2. Geology & Geochemistry Cluster, Department of Earth Sciences, VU Amsterdam, De Boelelaan 1085, 1081 HV Amsterdam, The Netherlands

3. Key Laboratory of Tectonics and Petroleum Resources, Ministry of Education, China University of Geosciences, Wuhan 430074, China

4. State Key Laboratory of Isotope Geochemistry, Guangzhou Institute of Geochemistry, Chinese Academy of Sciences, Guangzhou 510640, China

 Rong-Guo Hu: <https://orcid.org/0000-0003-4750-8541>;  Hua-Ning Qiu: <https://orcid.org/0000-0002-4971-3664>

ABSTRACT: The joint methods of $^{40}\text{Ar}/^{39}\text{Ar}$ laser stepwise heating and *in vacuo* crushing have been applied to date amphiboles from the North Qaidam ultra-high pressure metamorphic amphibolites. Two amphibole samples analyzed by laser heating yielded saddle-shaped age spectra with total gas ages of 574.5 ± 2.5 and 562.5 ± 2.5 Ma. These ages are much older than the reported zircon U-Pb ages (~ 495 Ma) from Yuka eclogite, indicating the presence of excess ^{40}Ar . In order to decipher the occurrence of excess ^{40}Ar and constrain the age of amphibolite-facies retrogression, two duplicate amphibole samples were further employed for $^{40}\text{Ar}/^{39}\text{Ar}$ *in vacuo* crushing analyses. Both samples exhibit similar monotonically declining release spectra, which are characterized by rapid decline of anomalously old apparent ages in the early steps. The data of the late steps yielded concordant apparent ages with plateau ages of 460.9 ± 1.2 and 459.6 ± 1.8 Ma. We interpret that gases released in the early steps derive from the significant excess ^{40}Ar containing secondary fluid inclusions (SFIs) due to their distribution characteristics along cracks leading to be easily extracted, whereas those released in the later steps represent the contribution of the small primary fluid inclusions (PFIs).

KEY WORDS: $^{40}\text{Ar}/^{39}\text{Ar}$ dating, *in vacuo* crushing, amphibole, fluid inclusions.

0 INTRODUCTION

Amphibole is one of the most common minerals dated by the $^{40}\text{Ar}/^{39}\text{Ar}$ method due to its relatively high retentivity for argon and widespread occurrence in metamorphic and igneous rocks (e.g., McDougall and Harrison, 1999). In Yuka terrane, amphibole widely occurs in high/ultrahigh pressure (HP/UHP) metamorphic rocks (Hu et al., 2015b; Zhang et al., 2005). However, there are only rare $^{40}\text{Ar}/^{39}\text{Ar}$ works which have been devoted to amphibole in this terrane thus far. Possible reasons include metamorphic amphibole is easily contaminated by excess ^{40}Ar (Hu et al., 2016; Di Vincenzo and Palmeri, 2001; Wartho et al., 1996; Cumbest et al., 1994; Blanckenburg and Villa, 1988; Harrison and McDougall, 1981), which is results

from complex release patterns and meaningless geological ages from the conventional stepwise heating analyses.

In this paper, amphibole separates from two amphibolites have been investigated by combined methods of $^{40}\text{Ar}/^{39}\text{Ar}$ laser stepwise heating and *in vacuo* crushing. Noble gases in fluid inclusions can be effectively liberated by *in vacuo* crushing method has been widely accepted (Hu et al., 2015b; Jiang et al., 2012; Qiu and Wijbrans, 2008; Kendrick et al., 2001; Turner and Wang, 1992; Kelley et al., 1986). Nevertheless, whether significant quantities of lattice-hosted noble gases could be extracted via protracted *in vacuo* crushing experiments is still an active research (Uunk et al., 2017; Hu et al., 2015a; Bai et al., 2013; Kendrick et al., 2011; Kendrick and Phillips, 2009a, b; Qiu and Wijbrans, 2009). Here, according to the comparable results from these two methods, we attempt to (1) assess whether the sample contains excess ^{40}Ar ; if excess ^{40}Ar existing, decipher its possible occurrence; (2) constrain the timing of fluid flow and amphibolite-facies retrogression of Yuka eclogite, and (3) discuss if protracted *in vacuo* crushing can extract substantive amount of argon gases from the crystal lattice.

*Corresponding author: hurongguo@163.com;
huaning.qiu@gmail.com

© China University of Geosciences and Springer-Verlag GmbH Germany, Part of Springer Nature 2018

Manuscript received March 15, 2017.

Manuscript accepted August 5, 2017.

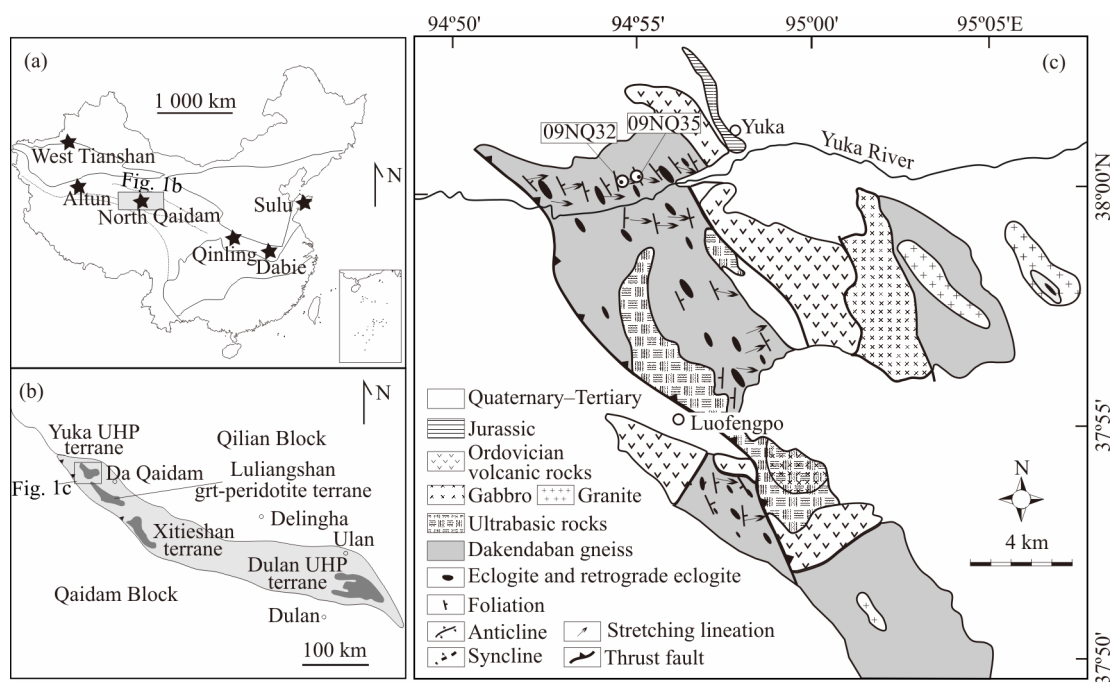


Figure 1. (a) Geological sketch map showing the locality of North Qaidam Orogen in China (modified after <http://bzdt.nasg.gov.cn/index.jsp> No. GS (2016) 1595); (b) sketch map showing distribution of UHP metamorphic terranes in the North Qaidam orogenic belt; (c) sketch map showing the Yuka terrane and sample localities (modified after Zhang et al., 2005).

1 GEOLOGICAL SETTING

The North Qaidam orogenic belt, parallel to the North Qilian suture zone, is located at the northern margin of the Qaidam Block of NW China (Fig. 1a). This UHP metamorphic belt is the second known occurrence of coesite/diamond in deep crustal rocks in China besides the Dabie-Sulu in central-eastern China (Yang et al., 2001), and records a complete history of the evolution of a continental orogen from initial oceanic subduction, through continental collision and subduction, to ultimate orogenic collapse in the time period from the Neoproterozoic to the Paleozoic (Song et al., 2014, 2005; Zhang et al., 2013). Geographically, it is bounded by the block (microplate) to the northeast, the Qaidam Block to the southwest, and it extends for around 400 km long along an NWW-strike from the Altyn-Tagh fault in the west to the Wahong-Shan fault in the east (Figs. 1a, 1b). Based on field occurrences, petrology and rock association, the North Qaidam UHP metamorphic belt can be subdivided into four sub-units, from east to west: the Dulan eclogite-gneiss terrane (DLT), the Xitieshan eclogite-gneiss terrane (XTT), the Luliangshan (garnet) peridotite-gneiss terrane (LLT), and the Yuka eclogite-gneiss terrane (YKT), which are separated by Paleozoic to Cenozoic sediments (Fig. 1b).

The Yuka eclogite-gneiss unit is located in the westernmost segment of the North Qaidam Orogen, western China (Fig. 1b). It mainly consists of gneisses, with coesite-bearing eclogite and amphibolite lenses up to a few meters across cropping out along the north bank of the Yuka River (Fig. 1c) (Song et al., 2014; Zhang et al., 2009; Chen et al., 2005). Peak metamorphic conditions were determined to be 566–730 °C and 2.9–3.2 GPa (Zhang G B et al., 2009; Zhang J X et al., 2005). The $^{40}\text{Ar}/^{39}\text{Ar}$ measurements on amphibole and phengite concentrated from the eclogites gave isochron ages of 477 ± 8

and 466 ± 5 Ma for cooling ages, respectively, and their isotope correlation diagrams indicated no excess ^{40}Ar within these minerals (Zhang et al., 2005). In contrast, using the $^{40}\text{Ar}/^{39}\text{Ar}$ stepwise heating method, Hu et al. (2014) and Menold et al. (2016) noticed that the eclogite phengites yielded anomalously old ages ranging from 534 to 750 Ma, implying the presence of extraneous ^{40}Ar , i.e., inherited or excess ^{40}Ar .

2 SAMPLES AND ANALYTICAL METHODS

The sample of gneissic amphibolite 09NQ32 was collected from the margin of an eclogite block in Yuka terrane, which mainly consists of quartz (20%–30%), phengite (20%–30%), amphibole (~15%), plagioclase (15%–25%), garnet (~5%) and zoisite (~5%) (see Fig. 2a). Amphiboles are classified into pargasite, barroisite and tschermakite (c.f., Leake et al., 1997), with 6 spot analyses giving K/Ca ratios ranging from 0.09 to 0.12 and a weighted-mean value of 0.11 ± 0.01 (see Table 1). Sample 09NQ35 was taken from a lens-shaped amphibolite block hosted by gneiss. It is characterized by medium- to coarse-grained massive structure, and consists of amphibole (~55%), chlorite (~10%), epidote (~10%), plagioclase (~5%), garnet (~5%), biotite (~5%), symplectites (Amp+Pl, ~5%) with minor titanite (see Fig. 2c). Amphiboles are classified into barroisite and magnesio-katophorite (c.f., Leake et al., 1997), with 6 spot analyses giving K/Ca ratios ranging from 0.06 to 0.09 and a weighted-mean value of 0.07 ± 0.01 (see Table 1). Petrographic observations have been carried out on polished thin section. Most of the fluid inclusions in the amphiboles are primary and small in size (0.5–3 μm), which are characterized by irregularly, tubular and elongated shapes, as well as random distribution (Figs. 2b, 2d). Since the small size, and what is more, relative high refractive index of amphibole prevents the determination of their chemical compositions

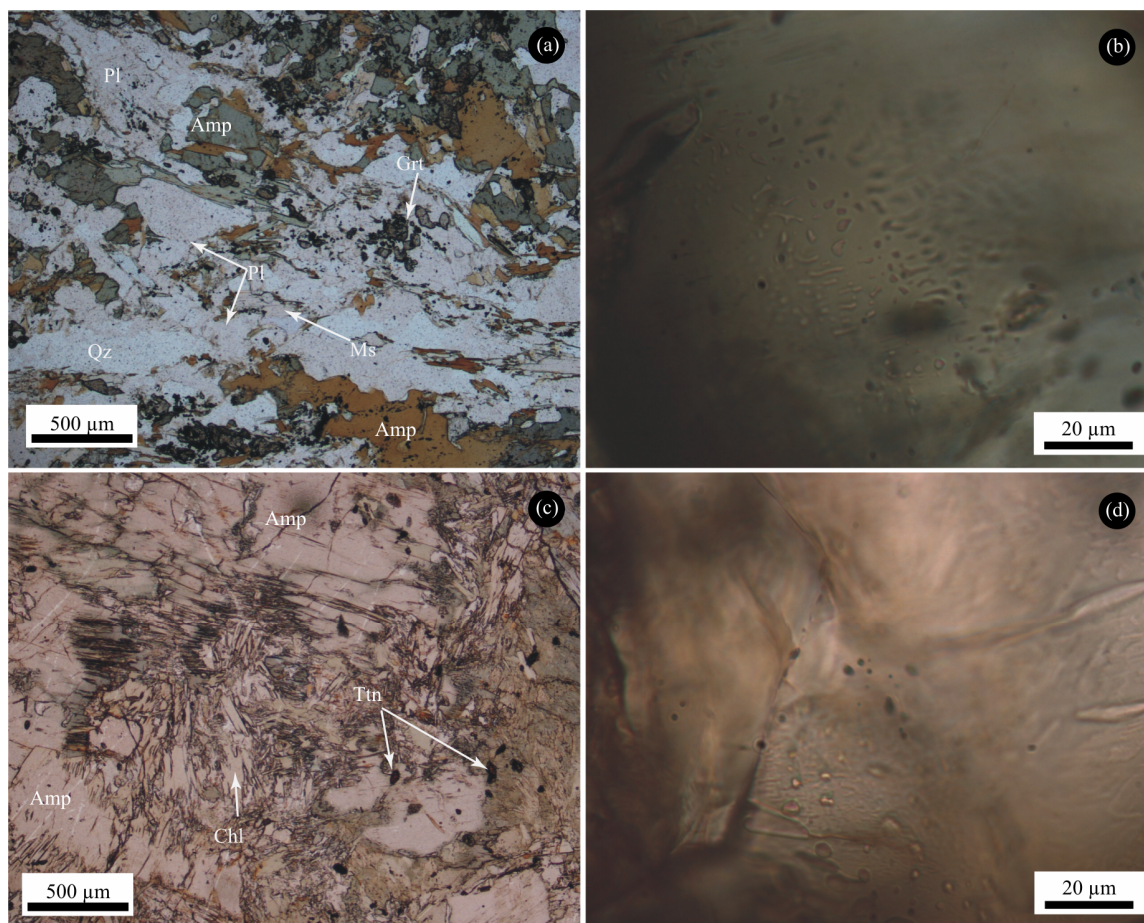


Figure 2. (a), (c) Photomicrographs showing paragenesis and texture of amphibolites 09NQ32 and 09NQ35; (b), (d) photomicrographs showing the primary fluid inclusions in amphiboles of 09NQ32 and 09NQ35, which are characterized by randomly distributed with irregularly, elongated and tubular in shapes.

and freezing/homogenization temperatures with a conventional heating-freezing stage.

Samples were crushed and sieved to obtain a size fraction of 250–500 μm . After magnetic separation, heavy liquid techniques were applied to separate amphibole. Finally, all the samples were hand-picked under the binocular microscope. Samples were wrapped in aluminum foil and loaded into quartz tubes together with standards and irradiated at the Oregon State University TRIGA Reactor in the cadmium shielded CLICIT facility. Irradiation times were 20 hrs for irradiation VU83. Correction factors for interfering argon isotopes derived from Ca and K isotopes are: $(^{39}\text{Ar}/^{37}\text{Ar})_{\text{Ca}}=0.000\ 673$, $(^{36}\text{Ar}/^{37}\text{Ar})_{\text{Ca}}=0.000\ 264$, $(^{40}\text{Ar}/^{39}\text{Ar})_{\text{K}}=0.000\ 86$ and $(^{38}\text{Ar}/^{39}\text{Ar})_{\text{K}}=0.012\ 11$. Flux monitor standards for J -value calculation for this project were DRA Sanidine with an assumed age of 25.26 ± 0.2 Ma (Wijbrans et al., 1995). The age of the standard Sanidine is compatible with the set of Renne et al. (1998), based on biotite GA1550 (at K/Ar age of 98.79 ± 0.69 Ma). Argon isotope ratios were measured on two different mass spectrometers in the VU University Amsterdam. Laser stepwise heating of amphibole crystals was achieved using a 50 W Synrad[®] 48-5 series CO₂ laser, connected with a MAP 215-50 mass spectrometer (Qiu and Wijbrans, 2006; Wijbrans et al., 1995). The gases released were purified by a Fe/V/Zr getter pump operated at 250 $^{\circ}\text{C}$ and a Zr/Al pump operated at 450 $^{\circ}\text{C}$. The blanks are: ^{36}Ar (0.000 6–0.008 6) mV, ^{37}Ar (0.000 04–0.000 13) mV, ^{38}Ar (0.000 2–0.001 8) mV, ^{39}Ar (0.000 1–

0.001 7) mV and ^{40}Ar (0.18–2.38) mV. Mass discrimination (1.002–1.010 per atomic mass unit) was monitored by frequent analysis of $^{40}\text{Ar}/^{38}\text{Ar}$ reference gas pipette aliquots. *In vacuo* crushing experiment was carried out in an in-house designed crushing apparatus that was connected to a three stage extraction line and a quadrupole mass spectrometer (Schneider et al., 2009). Samples were loaded into a 40 cm long, 4 cm diameter Inconel[®] tube and crushed by an iron pestle that is lifted and dropped with a frequency of one time per second (1 Hz) using external electromagnet-control. The extracted gases were exposed to a cold trap filled with liquid nitrogen (kept at ca. 0 $^{\circ}\text{C}$), and then purified at 250 $^{\circ}\text{C}$ by a Fe/V/Zr getter pump and 450 $^{\circ}\text{C}$ by a Zr/Al getter pump. The purification process lasted for around 16 min before the gas was analyzed for the argon isotopes in the mass spectrometer. The blanks are: ^{36}Ar (41–81) cps, ^{37}Ar (0.8–2.53) cps, ^{38}Ar (11–30) cps, ^{39}Ar (10–36) cps and ^{40}Ar (15 822–29 712) cps. Mass discrimination determined to be ~ 1.034 per atomic mass unit. Experiments began and ended with cold blank analyses to correct for system blanks with the procedure described above but without moving the pestle. The sensitivity of this two systems were measured using an HD-B1 biotite standard (3.364×10^{-10} mol/g radiogenic ^{40}Ar content) (Hess and Lippolt, 1994), which yielded average values of 2.87 A/mol for the MAP-215-50 mass spectrometer and 0.096 7 A/mol ($\pm 6.6\%$, 1σ) for the quadrupole mass spectrometer, respectively.

Table 1 Representative microprobe analyses data (wt.%) of amphibole (23O following Holland and Blundy, 1994)

Sample	09NQ32						09NQ35					
	37	38	48	53	52	43	64	80	100	119	120	85
Spot-position	Ts	Ts	Ts	Ts	Prg	Brs	Mktp	Mktp	Mktp	Brs	Brs	Brs
SiO ₂	44.08	44.08	44.97	44.41	43.86	45.27	48.98	46.48	45.48	51.08	51.09	51.45
TiO ₂	0.41	0.44	0.40	0.48	0.46	0.48	0.26	0.42	0.33	0.12	0.16	0.16
Al ₂ O ₃	15.22	15.51	15.38	15.75	15.34	16.45	13.40	15.04	15.60	12.21	12.33	12.50
FeO	14.38	14.18	13.57	13.97	14.68	14.09	8.17	9.33	10.09	7.68	6.88	7.49
MnO	0.24	0.21	0.12	0.12	0.22	0.21	0.04	0.00	0.05	0.02	0.03	0.02
MgO	10.54	10.15	10.83	10.85	10.13	9.47	13.56	12.52	11.98	13.98	14.32	14.06
CaO	10.70	10.06	9.93	9.73	9.96	8.22	7.28	8.22	7.95	6.23	6.27	6.29
Na ₂ O	2.30	2.58	2.82	2.91	2.66	3.49	4.88	4.66	4.76	5.05	5.19	5.25
K ₂ O	0.83	0.97	0.94	0.86	1.00	0.79	0.52	0.49	0.49	0.53	0.48	0.50
Total	98.71	98.18	98.95	99.08	98.29	98.46	97.08	97.16	96.74	96.89	96.74	97.70
Si	6.42	6.44	6.49	6.42	6.43	6.54	6.95	6.67	6.59	7.20	7.19	7.19
Al ^{IV}	1.53	1.51	1.46	1.53	1.52	1.40	1.02	1.28	1.38	0.78	0.79	0.79
Al ^{VI}	1.08	1.17	1.15	1.15	1.13	1.40	1.23	1.26	1.28	1.24	1.25	1.26
Ti	0.05	0.05	0.04	0.05	0.05	0.05	0.03	0.05	0.04	0.01	0.02	0.02
Mn	0.03	0.03	0.01	0.01	0.03	0.03	0.00	0.00	0.01	0.00	0.00	0.00
Mg	2.29	2.21	2.33	2.34	2.21	2.04	2.87	2.68	2.59	2.94	3.01	2.93
Ca	1.67	1.58	1.54	1.51	1.56	1.27	1.11	1.26	1.23	0.94	0.95	0.94
Na	0.65	0.73	0.79	0.81	0.75	0.98	1.34	1.30	1.34	1.38	1.42	1.42
K	0.15	0.18	0.17	0.16	0.19	0.15	0.09	0.09	0.09	0.10	0.09	0.09
Fe ³⁺	0.00	0.00	0.00	0.00	0.00	0.00	0.00	0.00	0.00	0.00	0.00	0.00
Fe ²⁺	1.75	1.73	1.64	1.69	1.80	1.70	0.97	1.12	1.22	0.91	0.81	0.87
Cations	15.63	15.63	15.64	15.67	15.67	15.56	15.61	15.71	15.76	15.51	15.52	15.52
K/Ca	0.092	0.115	0.113	0.105	0.119	0.114	0.071	0.060	0.062	0.085	0.076	0.079

The mineral compositions were analysed using a JEOL JXA-8800M electron microprobe at the Department of Earth Sciences at VU University Amsterdam. The analyses were performed using an accelerating voltage of 15.0 kV and a beam current of approximately 20 nA. Counting times were 20–30 s on peaks and half of this on backgrounds. The data were regressed using an oxide-ZAF correction program supplied by JEOL. Natural minerals were used as standards. Ts. tschermakite; Prg. pargasite; Brs. barroisite; Mktp. magnesio-katophorite.

3 $^{40}\text{Ar}/^{39}\text{Ar}$ DATING RESULTS

The $^{40}\text{Ar}/^{39}\text{Ar}$ dating results are calculated using the ArArCALC software package which was written by Koppers (2002). The $^{40}\text{Ar}/^{39}\text{Ar}$ analytical data are listed in Table 2. Age spectra and isochrones are plotted in Fig. 3. All errors are reported at a 2σ confidence level in the text and figures. In an attempt to search for elemental correlations, we performed multiple regressions on the amount of $^{40}\text{Ar}^*$, Cl ($^{38}\text{Ar}_{\text{Cl}}$) and K ($^{39}\text{Ar}_{\text{K}}$) with the aim of identifying the different Ar sources in the fluid inclusions (e.g., Menold et al., 2016; Bai et al., 2013; Smye et al., 2013; Jiang et al., 2012; Qiu and Wijbrans, 2006; Kendrick et al., 2001; Kelley et al., 1986). Here, $^{40}\text{Ar}^*$ denotes total ^{40}Ar just minus atmospheric ^{40}Ar ($^{40}\text{Ar}_{\text{A}}$). In other words, $^{40}\text{Ar}^*$ includes both K *in situ* decay derived radiogenic ^{40}Ar ($^{40}\text{Ar}_{\text{R}}$) and parentless excess ^{40}Ar ($^{40}\text{Ar}_{\text{E}}$).

Laser stepwise heating analyses of amphibole separates 09NQ32Amp and 09NQ35Amp exhibited similar complex release spectra, which are characterized by extremely high apparent ages in the initial steps (up to 0.9–1.2 Ga) and followed somewhat saddle-shaped released patterns of the left segment (480 to 610 Ma), with a total gas age of 574.5 ± 2.5 and 562.5 ± 2.5 Ma, respectively (Figs. 3a, 3c). On the argon three-

isotope plot, good correlations cannot be obtained because too many of the steps lie close to the $^{39}\text{Ar}/^{40}\text{Ar}$ axis (Figs. 3b, 3d).

During *in vacuo* crushing experiment, amphibole separates 09NQ32Amp underwent 35 stages, around 7 000 number of stokes. It yielded a monotonically decreasing staircase-shaped age spectrum characterized by anomalously high apparent ages in the initial steps (Fig. 3a). Subsequently, upon continued crushing, the apparent ages gradually stabilize to reveal age plateau x, with plateau age of 460.9 ± 1.2 Ma ($^{39}\text{Ar}_{\text{K}}=55.3\%$, MSWD=7.4). The data points of the steps defining the plateau age yield isochron with age of 457.6 ± 0.9 Ma (MSWD=3.1), corresponding to an initial $^{40}\text{Ar}/^{36}\text{Ar}$ ratio of 411 ± 27 (Fig. 3b). Sample 09NQ35Amp was subjected to 24 crushing steps of around 6 000 impacts, and produced a descending staircase-shaped age spectrum. Apparent ages decrease from as old as 3 075 to 494 Ma with steps 1 to 14, and then formed a relative flat age spectrum from stages 15 to 24 with a plateau age of 459.6 ± 1.8 Ma ($^{39}\text{Ar}_{\text{K}}=54.2\%$, MSWD=5.9) (Fig. 3c). The data points defining the age plateau x yield a well-defined isochron with age of 458.0 ± 1.9 Ma (MSWD=5.7), corresponding to an initial $^{40}\text{Ar}/^{36}\text{Ar}$ ratio of 540.7 ± 18.9 (Fig. 3d).

Table 2 $^{40}\text{Ar}/^{39}\text{Ar}$ dating data

Step	Laser power	$^{36}\text{Ar}_{\text{Air}}$	$^{37}\text{Ar}_{\text{Ca}}$	$^{38}\text{Ar}_{\text{Cl}}$	$^{39}\text{Ar}_{\text{K}}$	$^{40}\text{Ar}^*$	Age (Ma)	$^{40}\text{Ar}^*$ (%)	$^{39}\text{Ar}_{\text{K}}$ (%)	K/Ca
Amphibole 09NQ32Amp by laser step heating, $J=0.004\ 821\ 16$, $I_0=295.5$, Yuka terrane										
1	0.20 W	0.057 0	0.196 4	0.000 5	0.162 9	29.791 5	1 140.4±8.1	63.88	0.47	0.357±0.250
2	0.24 W	0.025 4	0.577 7	0.000 8	0.542 1	51.103 9	675.9±2.5	87.21	1.58	0.404±0.111
3	0.30 W	0.015 3	3.314 9	0.001 9	1.754 6	137.434 3	578.0±1.7	96.81	5.10	0.228±0.097
4	0.35 W	0.009 3	7.382 1	0.003 6	3.015 4	232.421 6	570.1±1.3	98.84	8.77	0.176±0.030
5	0.39 W	0.009 6	7.027 9	0.006 8	3.293 1	264.477 5	590.5±1.4	98.94	9.57	0.201±0.065
6	0.42 W	0.006 5	6.803 8	0.006 6	2.373 7	189.786 5	588.2±1.6	98.99	6.90	0.150±0.047
7	0.45 W	0.007 3	9.529 6	0.008 7	2.659 8	214.848 6	593.3±2.0	99.00	7.73	0.120±0.031
8	0.48 W	0.009 3	9.831 7	0.010 1	2.956 7	238.321 0	592.3±2.7	98.86	8.60	0.129±0.035
9	0.52 W	0.006 9	6.574 9	0.008 2	2.270 8	178.638 7	580.1±1.4	98.86	6.60	0.149±0.040
10	0.56 W	0.006 1	4.708 1	0.007 1	1.940 7	149.425 5	569.5±1.6	98.82	5.64	0.177±0.070
11	0.60 W	0.003 9	4.978 1	0.005 1	1.430 5	105.949 9	550.9±1.1	98.92	4.16	0.124±0.022
12	0.65 W	0.006 1	5.679 5	0.006 6	1.827 5	140.517 1	568.9±1.5	98.74	5.31	0.138±0.067
13	0.70 W	0.004 0	5.620 5	0.004 7	1.370 5	102.311 0	554.6±1.3	98.86	3.98	0.105±0.019
14	0.75 W	0.002 9	5.941 5	0.005 5	1.374 6	105.209 4	566.6±2.0	99.18	4.00	0.099±0.019
15	0.85 W	0.003 1	5.936 6	0.006 1	1.491 1	113.607 7	564.4±1.6	99.21	4.34	0.108±0.020
16	1.00 W	0.002 5	6.102 5	0.006 0	1.540 8	115.160 4	555.2±1.3	99.37	4.48	0.109±0.022
17	1.30 W	0.003 5	8.345 7	0.008 0	2.185 2	177.191 0	595.3±1.7	99.42	6.35	0.113±0.037
18	1.60 W	0.002 6	7.942 1	0.006 6	1.615 1	134.327 6	608.3±1.9	99.43	4.70	0.087±0.036
19	2.00 W	0.001 0	2.839 9	0.002 7	0.589 7	49.033 4	608.1±1.7	99.38	1.71	0.089±0.020
Amphibole 09NQ35Amp by Laser step heating, $J=0.004\ 912\ 1$, $I_0=295.5$, Yuka terrane										
1	0.24 W	0.013 5	0.964 4	0.000 8	0.151 6	20.416 1	916.1±3.4	83.62	0.52	0.068±0.013
2	0.30 W	0.015 4	3.353 7	0.002 4	0.526 7	52.373 8	717.5±2.0	92.01	1.82	0.068±0.012
3	0.35 W	0.009 5	7.077 7	0.004 0	1.501 2	124.796 6	617.8±1.5	97.81	5.20	0.091±0.015
4	0.39 W	0.008 3	9.874 1	0.001 3	1.918 1	161.301 8	623.8±2.8	98.51	6.64	0.084±0.016
5	0.42 W	0.007 8	16.222 7	0.015 8	2.955 2	248.240 1	623.2±2.3	99.08	10.23	0.078±0.014
6	0.45 W	0.008 2	14.431 1	0.005 6	2.306 4	167.134 1	549.4±1.6	98.57	7.98	0.069±0.014
7	0.48 W	0.007 7	10.926 3	0.006 1	2.162 4	155.446 4	545.6±2.7	98.57	7.48	0.085±0.023
8	0.52 W	0.007 2	13.323 3	0.005 2	2.253 2	169.350 8	566.9±1.7	98.75	7.80	0.073±0.014
9	0.56 W	0.014 5	13.561 9	0.005 9	2.054 8	153.784 0	564.8±1.8	97.30	7.11	0.065±0.012
10	0.60 W	0.005 8	12.193 2	0.009 4	2.206 3	152.328 6	526.8±1.5	98.89	7.64	0.078±0.018
11	0.65 W	0.004 2	10.975 9	0.008 7	2.293 8	144.892 7	487.5±1.5	99.15	7.94	0.090±0.015
12	0.70 W	0.007 0	9.050 8	0.005 8	1.824 6	126.067 8	527.2±1.8	98.39	6.32	0.087±0.029
13	0.75 W	0.004 2	7.659 2	0.009 4	1.612 0	108.290 8	514.5±2.0	98.85	5.58	0.091±0.016
14	0.85 W	0.002 8	5.869 8	0.000 9	0.982 9	68.648 2	532.1±3.5	98.79	3.40	0.072±0.013
15	1.00 W	0.004 0	7.507 1	0.000 5	1.410 1	88.270 8	483.7±2.6	98.68	4.88	0.081±0.015
16	1.30 W	0.005 3	9.572 2	0.001 1	1.741 3	137.682 4	592.0±2.8	98.87	6.03	0.078±0.015
17	1.60 W	0.003 4	5.302 3	0.004 6	0.993 0	73.104 3	556.9±2.0	98.66	3.44	0.081±0.015

Note: These $^{40}\text{Ar}/^{39}\text{Ar}$ experiments were measured using an MAP215-50 mass spectrometer in VU University Amsterdam. The MAP-215-50 had been fitted with a SEV-217 electron multiplier with the amplifier equipped with three resistors of 10^9 , 10^8 and $10^7\ \Omega$ that are automatically switched by the computer according to the ^{40}Ar signal intensities during peak-centering on the gas before analysis. Laser step heating was achieved with a 50 W Synrad 48-5 series CO_2 laser, using a Raylase industrial scan head as a beam diffuser by application of a triangular current on the y -axis motor drive of the scan head. The argon isotopes are listed in volt.

Table 2 Continued

Step	Pestle drop number	$^{36}\text{Ar}_{\text{Air}}$	$^{37}\text{Ar}_{\text{Ca}}$	$^{38}\text{Ar}_{\text{Cl}}$	$^{39}\text{Ar}_{\text{K}}$	$^{40}\text{Ar}^*$	Age (Ma)	$^{40}\text{Ar}^*$ (%)	$^{39}\text{Ar}_{\text{K}}$ (%)	K/Ca
Amphibole 09NQ32Amp by <i>in vacuo</i> crushing, $J=0.004$ 821 16, $I_0=295.5$, Yuka terrane										
1	6	26.08	336.82	5.76	275.07	321	3 415.4±40.0	97.66	0.09	0.351±0.186
2	12	25.32	610.25	8.08	527.91	462	2 983.3±11.7	98.41	0.18	0.372±0.131
3	20	30.94	1 123.65	11.63	946.25	710	2 761.7±10.6	98.73	0.32	0.362±0.080
4	30	15.24	1 351.68	12.98	1 415.99	688	2 178.5±8.8	99.35	0.48	0.450±0.073
5	40	128.73	1 759.65	15.03	1 959.81	700	1 806.9±5.0	94.85	0.67	0.479±0.128
6	50	68.82	2 396.01	10.54	2 572.64	620	1 392.1±5.7	96.83	0.88	0.462±0.074
7	60	61.93	2 933.41	9.43	3 197.30	734	1 344.5±3.4	97.57	1.09	0.469±0.060
8	80	57.21	3 331.95	9.68	3 781.34	782	1 248.1±3.1	97.88	1.29	0.488±0.056
9	100	48.48	3 689.38	3.47	4 936.09	681	920.4±2.5	97.94	1.68	0.575±0.068
10	120	79.30	4 876.59	15.50	5 715.07	806	936.4±3.2	97.18	1.95	0.504±0.053
11	130	79.60	4 255.97	7.56	5 795.70	834	951.1±4.8	97.26	1.97	0.586±0.068
12	150	57.63	4 221.73	8.44	6 514.03	702	755.3±2.9	97.63	2.22	0.663±0.088
13	150	40.26	4 884.78	14.51	6 974.35	655	674.5±1.7	98.22	2.38	0.614±0.074
14	160	18.57	6 103.76	12.33	8 657.66	703	596.7±2.7	99.23	2.95	0.610±0.083
15	180	40.29	5 745.36	5.03	8 844.08	648	546.1±1.5	98.20	3.01	0.662±0.074
16	200	41.49	5 497.41	16.64	10 554.92	757	536.1±1.5	98.41	3.60	0.826±0.095
17	210	6.27	4 978.29	2.71	9 698.33	649	504.5±1.6	99.71	3.30	0.838±0.100
18	230	26.27	5 398.56	11.25	11 789.81	751	483.5±1.4	98.98	4.02	0.939±0.105
19	250	180.30	6 185.42	10.67	12 435.52	792	483.3±0.9	93.70	4.24	0.864±0.111
20	270	51.92	7 043.99	14.85	12 188.73	769	479.3±1.8	98.04	4.15	0.744±0.075
21	280	52.48	6 118.81	17.05	12 481.59	782	476.3±1.7	98.05	4.25	0.877±0.089
22*	300	49.82	6 396.30	7.49	12 940.88	783	461.8±1.7	98.15	4.41	0.870±0.102
23*	300	76.80	6 852.33	8.21	13 114.90	795	462.7±1.6	97.22	4.47	0.823±0.103
24*	320	60.56	6 162.39	4.92	12 863.30	777	461.4±1.1	97.75	4.38	0.898±0.102
25*	320	54.90	6 462.83	9.23	12 205.35	737	461.5±1.2	97.85	4.16	0.812±0.115
26*	330	67.76	7 066.10	7.87	13 490.76	816	462.1±0.9	97.61	4.60	0.821±0.098
27*	350	41.95	7 170.88	17.94	14 086.11	844	458.2±0.9	98.55	4.80	0.845±0.110
28*	370	30.07	7 279.17	19.51	13 022.61	785	460.6±1.1	98.88	4.44	0.769±0.105
29*	370	28.09	7 037.63	13.14	12 311.27	739	459.0±1.5	98.89	4.19	0.752±0.085
30*	390	33.05	6 117.90	6.86	11 124.22	670	460.5±1.0	98.56	3.79	0.782±0.102
31*	400	85.87	6 382.05	20.74	11 474.05	696	463.3±0.9	96.49	3.91	0.773±0.102
32*	370	49.34	5 782.71	11.71	9 331.55	561	459.2±1.4	97.47	3.18	0.694±0.091
33*	400	34.65	6 573.88	2.19	9 592.19	578	460.7±1.3	98.26	3.27	0.627±0.072
34*	400	41.09	5 527.88	11.63	7 719.24	466	460.9±1.5	97.46	2.63	0.600±0.071
35*	450	36.29	6 947.31	2.63	9 023.92	545	461.6±1.6	98.07	3.07	0.559±0.062
Amphibole 09NQ35Amp by <i>in vacuo</i> crushing, $J=0.004$ 912 1, $I_0=295.5$, Yuka terrane										
1	6	93.01	1 601.46	12.22	564.91	517	3 075.4±13.8	91.45	0.88	0.152±0.037
2	12	75.97	2 542.08	14.34	915.06	613	2 628.5±7.3	93.95	1.43	0.155±0.027
3	20	59.92	3 308.76	8.02	885.69	432	2 208.1±9.1	93.28	1.38	0.115±0.015
4	30	98.34	3 241.67	9.17	1 027.14	574	2 383.7±6.0	91.83	1.60	0.136±0.028
5	40	163.02	4 409.39	7.53	1 909.97	508	1 507.8±5.9	85.70	2.98	0.186±0.031

Table 2 Continued

Step	Pestle drop number	$^{36}\text{Ar}_{\text{Air}}$	$^{37}\text{Ar}_{\text{Ca}}$	$^{38}\text{Ar}_{\text{Cl}}$	$^{39}\text{Ar}_{\text{K}}$	$^{40}\text{Ar}^*$	Age (Ma)	$^{40}\text{Ar}^*$ (%)	$^{39}\text{Ar}_{\text{K}}$ (%)	K/Ca
Amphibole 09NQ35Amp by <i>in vacuo</i> crushing, $J=0.004\ 912\ 1$, $I_0=295.5$, Yuka terrane										
6	50	107.36	6 149.62	8.40	1 907.59	574 097.77	1 637.4±6.0	91.14	2.98	0.133±0.017
7	60	99.68	7 924.47	4.02	2 369.90	553 117.63	1 378±5.2	91.43	3.70	0.129±0.015
8	80	46.28	3 791.40	4.11	1 071.45	148 866.87	938.6±10.2	86.08	1.67	0.122±0.016
9	100	63.31	7 060.98	4.02	2 344.99	296 449.27	871.4±5.8	90.00	3.66	0.143±0.015
10	120	60.47	8 689.82	5.01	2 795.61	317 360.29	799.5±3.6	90.98	4.37	0.138±0.016
11	200	58.97	9 601.52	2.94	3 390.20	311 658.78	672.3±3.5	91.04	5.30	0.152±0.019
12	200	66.53	9 901.85	7.10	3 538.94	273 317.21	580.2±3.5	88.76	5.53	0.154±0.017
13	250	69.39	7 010.75	3.23	2 591.69	184 134.39	540.1±4.6	83.61	4.05	0.159±0.021
14	250	61.98	11 218.25	3.35	4 009.09	257 168.96	494.2±2.3	88.86	6.26	0.154±0.017
15*	300	67.79	11 696.06	9.08	4 171.94	247 504.75	461.4±1.5	87.53	6.52	0.153±0.020
16*	300	81.93	12 934.46	2.07	4 422.89	260 321.04	458.2±1.5	85.94	6.91	0.147±0.017
17*	350	65.60	12 842.53	2.32	4 435.36	262 842.74	460.9±1.9	88.51	6.93	0.149±0.018
18*	350	46.95	12 268.32	6.31	3 988.84	237 194.35	462.3±2.7	90.67	6.23	0.140±0.016
19*	400	27.65	6 908.29	5.35	2 501.61	147 769.00	459.6±2.4	91.13	3.91	0.156±0.019
20*	500	18.50	10 695.55	2.30	3 651.69	216 729.99	461.5±1.9	95.75	5.71	0.147±0.018
21*	550	19.35	9 460.26	5.99	2 998.80	179 683.30	465.4±3.9	94.70	4.69	0.136±0.016
22*	600	7.41	9 990.02	3.22	2 925.70	171 599.50	456.7±2.3	97.80	4.57	0.126±0.015
23*	600	6.32	9 450.66	1.18	2 806.67	164 045.53	455.3±2.3	98.03	4.39	0.128±0.018
24*	650	9.07	10 322.64	1.33	2 772.37	162 629.72	456.8±2.8	97.18	4.33	0.115±0.014

Note: These $^{40}\text{Ar}/^{39}\text{Ar}$ experiments were measured using a quadrupole mass spectrometer in VU Amsterdam. The argon isotopes are listed in “cps”. Data marked with “*” were included in the calculations for the isochron ages.

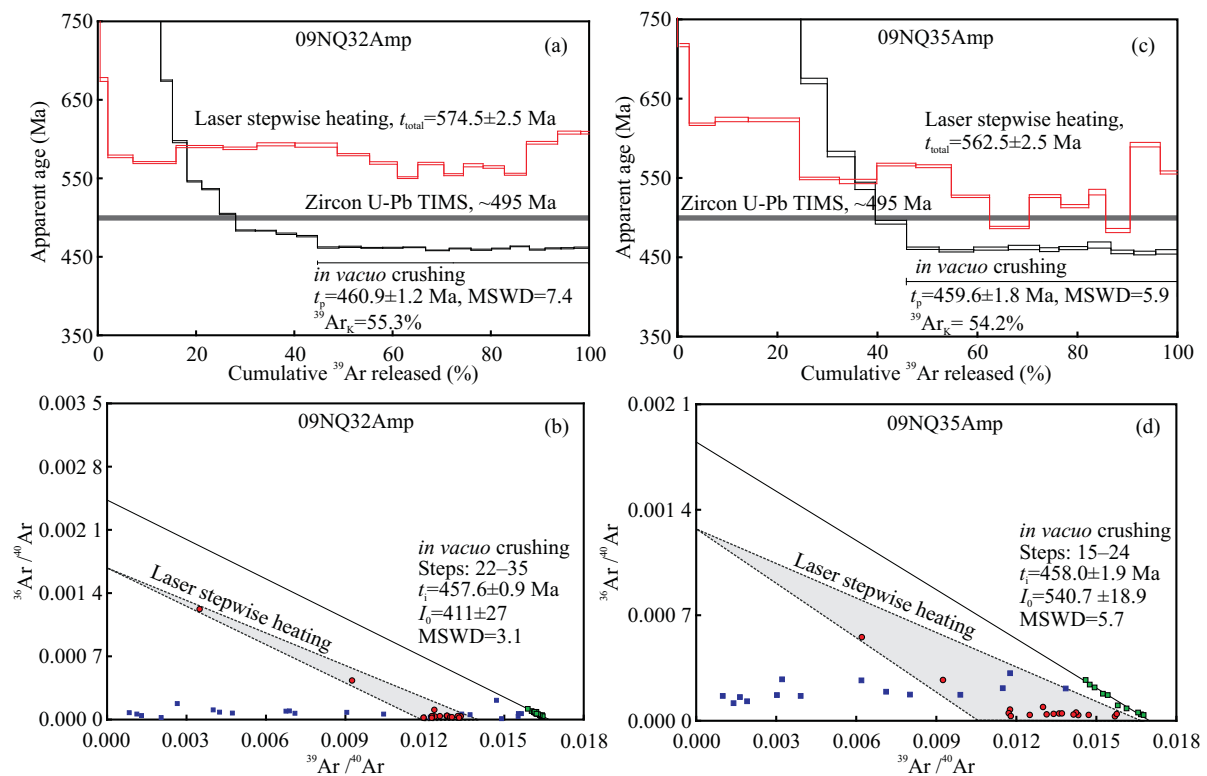


Figure 3. Age spectra (a), (c) and inverse isochrons (b), (d) of amphibole samples 09NQ32Amp and 09NQ35Amp by laser stepwise heating and *in vacuo* crushing. The U-Pb zircon metamorphic ages of Yuka eclogite from Zhang et al. (2005) are shown for comparison.

4 DISCUSSION

In Yuka terrane, eclogite zircons dated using the TIMS and LA-ICP-MS U-Pb methods gave what were interpreted to be eclogite-facies metamorphic ages of 436–495 Ma (Chen et al., 2009; Zhang et al., 2005). In this study, amphibole separates 09NQ32Amp and 09NQ35Amp by laser stepwise heating yielded similar saddle-shaped $^{40}\text{Ar}/^{39}\text{Ar}$ age spectra, which is usually considered to be indicative of the contamination of excess ^{40}Ar (e.g., Zeitler and Fitz Gerald, 1986; Harrison and McDougall, 1981; Lanphere and Brent Dalrymple, 1976). As shown in Fig. 3 and Table 2, these amphibole samples yielded total gas ages of 575–563 Ma and apparent ages ranging from 480 to 1 200 Ma, much older than the maximum zircon U-Pb result. It is unreasonable that an amphibole should give older $^{40}\text{Ar}/^{39}\text{Ar}$ ages than zircon U-Pb ages since the latter features with higher closure temperature, unless it contains excess ^{40}Ar . Excess ^{40}Ar diffusion from the grain-margins nearby ‘cation’ sites at low-temperature steps is one possible reason for steep profile (Zeitler and Fitz Gerald, 1986). Alternatively, excess ^{40}Ar released from the fluid inclusions at low temperatures is the other one (Kelley, 2002; Burgess et al., 1992).

The new results from amphibole samples $^{40}\text{Ar}/^{39}\text{Ar}$ *in vacuo* crushing analyses yielded similar descending staircase-shaped age spectra with anomalously high apparent ages in the first few steps and relative flat age plateau over the last several steps (Figs. 3a, 3c). For initial high apparent ages, following the interpretation of Hua-Ning Qiu and co-workers (e.g., Qiu and Wijbrans, 2008, 2006), the SFIs can be easily liberated during the early crushing steps, due to their relatively large volume and distribution characteristics along crack. In contrast, the PFIs are isolated and randomly distributed in host crystals, only can be extracted with more impacts. Thus, we suggest that the extremely high initial apparent ages should be contributed by the largest, most easily crushed secondary fluid inclusions (SFIs) that are dominated by excess ^{40}Ar and that were most likely incorporated in the amphibole after the initial amphibolite-facies conditions or even later. Because the cumulative release of radiogenic ^{40}Ar from the protolith that was degassed during metamorphism normally resulted in high concentrations of excess ^{40}Ar at the grain boundaries (Kelley, 2002). As a consequence, once escaped from the crystalline

reservoir it was dissolved in the fluid phase that was trapped in rocks during UHP metamorphism or later retrogression stages. Meanwhile, as shown in Fig. 4 ($^{40}\text{Ar}^*/^{39}\text{Ar}_K$ vs. $^{38}\text{Ar}_{Cl}/^{39}\text{Ar}_K$), the $^{40}\text{Ar}^*$ (represent $^{40}\text{Ar}_R + ^{40}\text{Ar}_E$) in good correlation with the $^{38}\text{Ar}_{Cl}$ in the initial crushing steps, implying the excess ^{40}Ar in the SFIs and CI are from the same source (Bai et al., 2013; Jiang et al., 2012; Turner and Wang, 1992). With continued crushing, the apparent ages decrease gradually probably reflecting a mixture between SFIs with excess ^{40}Ar and PFIs. Finally, once the high-excess ^{40}Ar reservoir is exhausted, subsequent gas components are mainly derived from smaller PFIs. During this stage of the experiment a relative flat age plateau is formed over the final several steps. The amphibole data points constituting the age plateaus result in isochrons with relative younger intercept ages (ca. 458 Ma), corresponding to initial $^{40}\text{Ar}/^{36}\text{Ar}$ values of ~411 to ~541, implying excess ^{40}Ar is also present in the fine PFIs of amphibole samples.

Previous studies have shown that crushing has little effect on the gas trapped within the crystal lattice (Qiu and Wijbrans, 2008, 2006; Dunlap and Kronenberg, 2001). In other words, the purpose of the crushing *in vacuo* technique is to extract the gas that was trapped in fluid inclusions and along cracks and cavities in crystals. Nevertheless, applying the *in vacuo* crushing method on scapolite gem, Kendrick and Phillips (2009b) argued that significantly amount of lattice-hosted noble gas can be liberated by prolonged crushing (about 96 000 crushing strokes). Thereby, the flat age plateau was probably interpreted to be: (1) gases contributed by crystal lattice release Ar components and (2) gases components may have derived from the smaller PFIs.

Here, we utilize the chemical components such as K ($^{39}\text{Ar}_K$) and Ca ($^{37}\text{Ar}_{Ca}$) and their ratios in fluid inclusions (by crushing) to decipher the possible argon reservoirs contributing to degassing since they are remarkably different from those of the solid phase (by laser stepwise heating or EMP analyses) (Jiang et al., 2012; Villa, 2001; Turner and Wang, 1992; Kelley et al., 1986). If the first hypothesis is true: the gases for the flat plateau that were derived from the lattice-hosted Ar, the weighted-mean K/Ca ratios of these steps should be consistent with those values from laser stepwise heating as well as from EMP analyses. Nevertheless, for Sample 09NQ32Amp, as

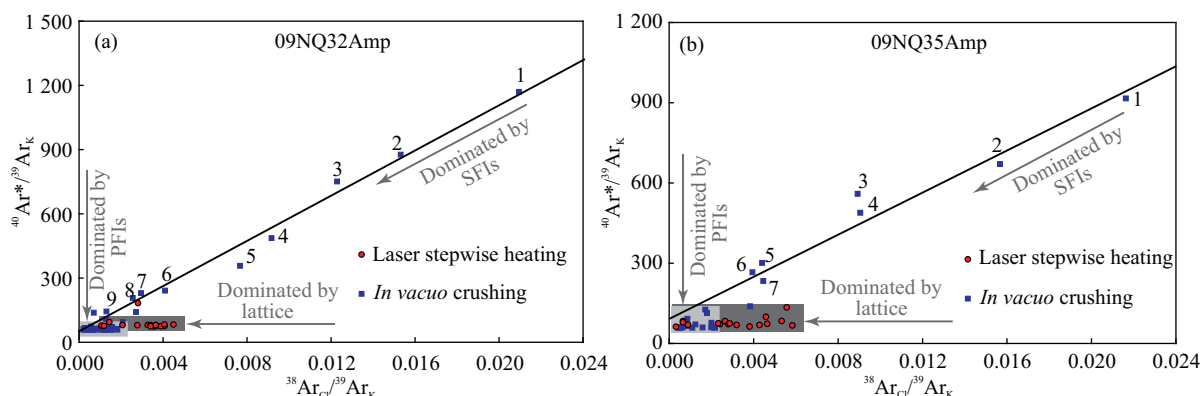


Figure 4. Plot of $^{40}\text{Ar}^*/^{39}\text{Ar}_K$ vs. $^{38}\text{Ar}_{Cl}/^{39}\text{Ar}_K$ based on the laser stepwise heating and *in vacuo* crushing data of the amphiboles 09NQ32Amp (a) and 09NQ35Amp (b). Crushing steps of the first few steps were numbered to show the sequence of crushing which dominated by secondary fluid inclusions (SFIs) and showing good correlation.

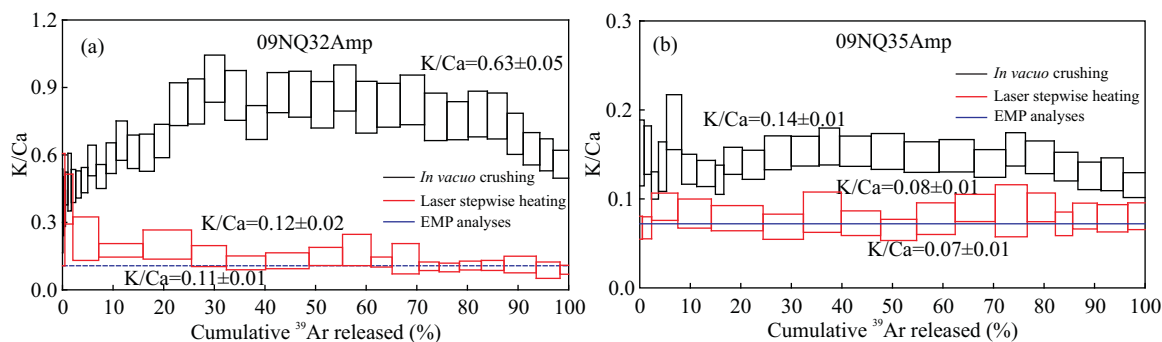


Figure 5. Weighted-mean K/Ca ratio spectra of amphibole samples 09NQ32Amp (a) and 09NQ35Amp (b) by *in vacuo* crushing and stepwise heating analyses. The distinct differences among K/Ca ratios indicate that the gases liberated by crushing and heating should come from different sources. The weighted-mean K/Ca ratios from EMP analyses are shown for comparison.

shown in Fig. 5a, the weighted-mean K/Ca spectrum for *in vacuo* crushing experiments is characterized by hump-shaped profile and remarkably higher K/Ca values (0.67 ± 0.05) than those laser stepwise heating (0.12 ± 0.02) or EMP analyses results (0.11 ± 0.01). Similar results are observed for Sample 09NQ35Amp as shown in Fig. 5b, its weighted-mean K/Ca ratios from *in vacuo* crushing (0.14 ± 0.01) are higher than the ratios from laser stepwise heating (0.08 ± 0.01) and EMP analyses (0.07 ± 0.01). Consequently, it seems unlikely that the around 6 000 to 7 000 number of stokes are enough to remove all fluid inclusions and only leave the solid phase argon to contribute to the degassing during late stages of crushing. Therefore, we consider the second postulate is the reasonable one. Moreover, the higher weighted-mean K/Ca values of the fluid inclusions also indicate they probably originated from dehydration and degassing of K-rich minerals (e.g., Cumbest et al., 1994).

It is well known that amphibole from HP/UHP rocks is mainly formed during amphibolite-facies retrogression. During this stage, significant amounts of fluid could be obtained from the molecular H₂O in nominally anhydrous minerals (e.g., garnet and omphacite), the breakdown of hydrous minerals (e.g., zoisite, phengite and lawsonite), the exsolution of hydroxyl minerals (Frezzotti et al., 2007; Zheng, 2004; Zheng et al., 2003), and even from the host gneiss (Zong et al., 2010; Chen et al., 2007). This kind of metamorphic fluid probably was trapped by amphibole crystals during crystallization and/or at a later stage by crack-seal mechanism. Such fluid inclusions can therefore be considered as PFIs. The ages of these PFIs therefore not only record aqueous fluid flow during the exhumation stages of HP/UHP rocks, but can also be taken as the best estimate for the ages of amphibolite facies retrogression.

Crushing experiments of two amphiboles yielded isochron ages of 457.6 ± 0.9 and 458.0 ± 1.9 Ma, respectively. These ages are concordant with the stepwise heating isochron ages (477–454 Ma) from Yuka phengite and amphibole that have been interpreted as the timing of early cooling in the eclogite facies after peak pressure metamorphism (Hu et al., 2014; Zhang et al., 2005). This suggests that the ⁴⁰Ar/³⁹Ar plateau ages and isochron ages of ca. 458 Ma of the amphibole samples constrain the age of fluid flow responsible for initial amphibolite-facies retrogression during the exhumation of the UHP rocks in Yuka terrane, North Qaidam.

5 CONCLUSION

The *in vacuo* crushing technique is an effective and promising approach to directly date the mineral formation ages in retrogressed HP/UHP rocks and decipher the occurrence of excess ⁴⁰Ar. Amphibole samples ⁴⁰Ar/³⁹Ar dating by *in vacuo* crushing indicate that the SFIs were formed subsequent to UHP metamorphism and that the amphibole incorporated significant amounts of heterogeneous excess ⁴⁰Ar in fluid inclusions. The excess ⁴⁰Ar is generally released early in the stepwise heating and crushing experiments. PFIs trapped during amphibole growth and released in the later stages of the crushing experiments contain relatively homogeneous excess ⁴⁰Ar. Moreover, lattice-hosted argon seems unlikely be released after undergone about 6 000–7 000 number of stokes. The isochron ages of ca. 458 Ma from crushing experiment reflects the timing of the amphibolite-facies retrogression during early stages of exhumation of the Yuka eclogite.

ACKNOWLEDGMENTS

We thank two anonymous reviewers for their comments that substantially improved this manuscript. We also sincerely thank Mr. Roel Van Elsas, Mrs. Wynanda Koot, Mr. Onno Postma, Mr. Arie Bikker, and Mr. Wim van der Plas from the VU Amsterdam, for their kind help in mineral separation, thin section preparation, and technical support for ⁴⁰Ar/³⁹Ar analyses. This work was funded by the National Natural Science Foundation of China (Nos. 41703054, 41503053), the Guangxi Natural Science Foundation Program (Nos. 2016GXNSFC380022, 2014GXNSFB118231) and the Chinese Academy of Sciences-Royal Netherlands Academy of Arts and Sciences Joint PhD Training Programme (No. O8PhD-08). The final publication is available at Springer via <https://doi.org/10.1007/s12583-017-0947-x>.

REFERENCES CITED

- Bai, X. J., Wang, M., Jiang, Y. D., et al., 2013. Direct Dating of Tin-Tungsten Mineralization of the Piaotang Tungsten Deposit, South China, by ⁴⁰Ar/³⁹Ar Progressive Crushing. *Geochimica et Cosmochimica Acta*, 114: 1–12. <https://doi.org/10.1016/j.gca.2013.03.022>
- Blanckenburg, F. V., Villa, I. M., 1988. Argon Retentivity and Argon Excess in Amphiboles from the Garbenschiefs of the Western Tauern Window, Eastern Alps. *Contributions to Mineralogy and Petrology*, 100(1): 1–11. <https://doi.org/10.1007/bf00399435>

- Burgess, R., Kelley, S. P., Parsons, I., et al., 1992. ^{40}Ar - ^{39}Ar Analysis of Perthite Microtextures and Fluid Inclusions in Alkali Feldspars from the Klokken Syenite, South Greenland. *Earth and Planetary Science Letters*, 109(1/2): 147–167. [https://doi.org/10.1016/0012-821x\(92\)90080-f](https://doi.org/10.1016/0012-821x(92)90080-f)
- Chen, D. L., Sun, Y., Liu, L., et al., 2005. Metamorphic Evolution of the Yuka Eclogite in the North Qaidam, NW China: Evidences from the Compositional Zonation of Garnet and Reaction Texture in the Rock. *Acta Petrologica Sinica*, 21(4): 1039–1048 (in Chinese with English Abstract)
- Chen, D. L., Liu, L., Sun, Y., et al., 2009. Geochemistry and Zircon U-Pb Dating and Its Implications of the Yukahe HP/UHP Terrane, the North Qaidam, NW China. *Journal of Asian Earth Sciences*, 35(3/4): 259–272. <https://doi.org/10.1016/j.jseaeas.2008.12.001>
- Chen, R. X., Zheng, Y. F., Gong, B., et al., 2007. Origin of Retrograde Fluid in Ultrahigh-Pressure Metamorphic Rocks: Constraints from Mineral Hydrogen Isotope and Water Content Changes in Eclogite-gneiss Transitions in the Sulu Orogen. *Geochimica et Cosmochimica Acta*, 71(9): 2299–2325. <https://doi.org/10.1016/j.gca.2007.02.012>
- Cumbest, R. J., Johnson, E. L., Onstott, T. C., 1994. Argon Composition of Metamorphic Fluids: Implications for $^{40}\text{Ar}/^{39}\text{Ar}$ Geochronology. *Geological Society of America Bulletin*, 106(7): 942–951. [https://doi.org/10.1130/0016-7606\(1994\)106<0942:acomfi>2.3.co;2](https://doi.org/10.1130/0016-7606(1994)106<0942:acomfi>2.3.co;2)
- Di Vincenzo, G., Palmeri, R., 2001. An ^{40}Ar - ^{39}Ar Investigation of High-Pressure Metamorphism and the Retrogressive History of Mafic Eclogites from the Lanterman Range (Antarctica): Evidence against a Simple Temperature Control on Argon Transport in Amphibole. *Contributions to Mineralogy and Petrology*, 141(1): 15–35. <https://doi.org/10.1007/s004100000226>
- Dunlap, W., Kronenberg, A., 2001. Argon Loss during Deformation of Micas: Constraints from Laboratory Deformation Experiments. *Contributions to Mineralogy and Petrology*, 141(2): 174–185. <https://doi.org/10.1007/s004100000217>
- Frezzotti, M. L., Ferrando, S., Dallai, L., et al., 2007. Intermediate Alkali-Alumino-Silicate Aqueous Solutions Released by Deeply Subducted Continental Crust: Fluid Evolution in UHP OH-Rich Topaz-Kyanite Quartzites from Donghai (Sulu, China). *Journal of Petrology*, 48(6): 1219–1241. <https://doi.org/10.1093/petrology/egm015>
- Harrison, T. M., McDougall, I., 1981. Excess ^{40}Ar in Metamorphic Rocks from Broken Hill, New South Wales: Implications for $^{40}\text{Ar}/^{39}\text{Ar}$ Age Spectra and the Thermal History of the Region. *Earth and Planetary Science Letters*, 55(1): 123–149. [https://doi.org/10.1016/0012-821x\(81\)90092-3](https://doi.org/10.1016/0012-821x(81)90092-3)
- Hess, J., Lippolt, H., 1994. Compilation of K-Ar measurements on HD-B1 Standard Biotite 1994 Status Report. Phanerozoic Time Scale. In: Odin, G. S., ed., IGCP Project. *Bulletin of Liaison and Informatics*, 12: 19–23
- Holland, T., Blundy, J., 1994. Non-Ideal Interactions in Calcic Amphiboles and Their Bearing on Amphibole-Plagioclase Thermometry. *Contributions to Mineralogy and Petrology*, 116(4): 433–447. <https://doi.org/10.1007/bf00310910>
- Hu, R. G., Qiu, H. N., Wijbrans, J. R., et al., 2014. $^{40}\text{Ar}/^{39}\text{Ar}$ Geochronology Study and the Genesis of Extraneous ^{40}Ar in Yuka HP/UHP Phengite, North Qaidam, NW China. *Earth Science Frontiers*, 21(1): 216–227 (in Chinese with English Abstract)
- Hu, R. G., Wijbran J. R., Brouwer F. M., et al., 2015a. Fluid Inclusions Study and Direct $^{40}\text{Ar}/^{39}\text{Ar}$ Dating by *in vacuo* Crushing of Quartz Veins within UHP Metamorphic Rocks from Yuka Terrane, North Qaidam Orogen, China. *Geochemical Journal*, 49(2): 139–155. <https://doi.org/10.2343/geochemj.2.0337>
- Hu, R. G., Wijbrans, J., Brouwer, F., et al., 2015b. Retrograde Metamorphism of the Eclogite in North Qaidam, Western China: Constraints by Joint $^{40}\text{Ar}/^{39}\text{Ar}$ *in vacuo* Crushing and Stepped Heating. *Geoscience Frontiers*, 6(5): 759–770. <https://doi.org/10.13039/501100001722>
- Hu, R. G., Wijbrans, J. R., Brouwer, F. M., et al., 2016. $^{40}\text{Ar}/^{39}\text{Ar}$ Thermochronological Constraints on the Retrogression and Exhumation of Ultra-High Pressure (UHP) Metamorphic Rocks from Xitieshan Terrane, North Qaidam, China. *Gondwana Research*, 36: 157–175. <https://doi.org/10.1016/j.gr.2016.04.009>
- Jiang, Y. D., Qiu, H. N., Xu, Y. G., 2012. Hydrothermal Fluids, Argon Isotopes and Mineralization Ages of the Fankou Pb-Zn Deposit in South China: Insights from Sphalerite $^{40}\text{Ar}/^{39}\text{Ar}$ Progressive Crushing. *Geochimica et Cosmochimica Acta*, 84: 369–379. <https://doi.org/10.1016/j.gca.2012.01.044>
- Kelley, S., Turner, G., Butterfield, A. W., et al., 1986. The Source and Significance of Argon Isotopes in Fluid Inclusions from Areas of Mineralization. *Earth and Planetary Science Letters*, 79(3/4): 303–318. [https://doi.org/10.1016/0012-821x\(86\)90187-1](https://doi.org/10.1016/0012-821x(86)90187-1)
- Kelley, S., 2002. Excess Argon in K-Ar and Ar-Ar Geochronology. *Chemical Geology*, 188(1/2): 1–22. [https://doi.org/10.1016/s0009-2541\(02\)00064-5](https://doi.org/10.1016/s0009-2541(02)00064-5)
- Kendrick, M. A., Burgess, R., Patrick, R. A. D., et al., 2001. Halogen and Ar-Ar Age Determinations of Inclusions within Quartz Veins from Porphyry Copper Deposits Using Complementary Noble Gas Extraction Techniques. *Chemical Geology*, 177(3/4): 351–370. [https://doi.org/10.1016/s0009-2541\(00\)00419-8](https://doi.org/10.1016/s0009-2541(00)00419-8)
- Kendrick, M. A., Phillips, D., 2009a. Discussion of ‘the Paleozoic Metamorphic History of the Central Orogenic Belt of China from $^{40}\text{Ar}/^{39}\text{Ar}$ Geochronology of Eclogite Garnet Fluid Inclusions by Qiu Hua-Ning and Wijbrans J.R.’. *Earth and Planetary Science Letters*, 279(3/4): 392–394. <https://doi.org/10.1016/j.epsl.2008.12.047>
- Kendrick, M. A., Phillips, D., 2009b. New Constraints on the Release of Noble Gases during *in vacuo* Crushing and Application to Scapolite Br-Cl-I and $^{40}\text{Ar}/^{39}\text{Ar}$ Age Determinations. *Geochimica et Cosmochimica Acta*, 73(19): 5673–5692. <https://doi.org/10.1016/j.gca.2009.06.032>
- Kendrick, M. A., Phillips, D., Wallace, M., et al., 2011. Halogens and Noble Gases in Sedimentary Formation Waters and Zn-Pb Deposits: A Case Study from the Lennard Shelf, Australia. *Applied Geochemistry*, 26(12): 2089–2100. <https://doi.org/10.1016/j.apgeochem.2011.07.007>
- Koppers, A. A. P., 2002. ArArCALC—Software for $^{40}\text{Ar}/^{39}\text{Ar}$ Age Calculations. *Computers & Geosciences*, 28(5): 605–619. [https://doi.org/10.1016/s0098-3004\(01\)00095-4](https://doi.org/10.1016/s0098-3004(01)00095-4)
- Lanphere, M. A., Brent Dalrymple, G., 1976. Identification of Excess ^{40}Ar by the $^{40}\text{Ar}/^{39}\text{Ar}$ Age Spectrum Technique. *Earth and Planetary Science Letters*, 32(2): 141–148. [https://doi.org/10.1016/0012-821x\(76\)90052-2](https://doi.org/10.1016/0012-821x(76)90052-2)
- Leake, B. E., Woolley, A. R., Arps, C. E. S., et al., 1997. Nomenclature of Amphiboles: Report of the Subcommittee on Amphiboles of the International Mineralogical Association, Commission on New Minerals and Mineral Names. *American Mineralogist*, 82(9/10): 1019–1037
- McDougall, I., Harrison, M., 1999. *Geochronology and Thermochronology by the $^{40}\text{Ar}/^{39}\text{Ar}$ Method*. Oxford University Press, New York. 269
- Menold, C. A., Grove, M., Sievers, N. E., et al., 2016. Argon, Oxygen, and Boron Isotopic Evidence Documenting $^{40}\text{Ar}_E$ Accumulation in Phengite during Water-Rich High-Pressure Subduction Metasomatism of Continental Crust. *Earth and Planetary Science Letters*, 446: 56–67. <https://doi.org/10.13039/1000000001>

- Qiu, H. N., Wijbrans, J. R., 2009. Reply to Comment by M. A. Kendrick and D. Phillips (2009) on "The Paleozoic Metamorphic History of the Central Orogenic Belt of China from $^{40}\text{Ar}/^{39}\text{Ar}$ Geochronology of Eclogite Garnet Fluid Inclusions" by Hua-Ning Qiu and J. R. Wijbrans (2008) [Earth Planet. Sci. Lett. 268 (2008) 501–514]. *Earth and Planetary Science Letters*, 279(3/4): 395–397. <https://doi.org/10.1016/j.epsl.2009.01.012>
- Qiu, H. N., Wijbrans, J. R., 2006. Paleozoic Ages and Excess ^{40}Ar in Garnets from the Bixiling Eclogite in Dabieshan, China: New Insights from $^{40}\text{Ar}/^{39}\text{Ar}$ Dating by Stepwise Crushing. *Geochimica et Cosmochimica Acta*, 70(9): 2354–2370. <https://doi.org/10.1016/j.gca.2005.11.030>
- Qiu, H. N., Wijbrans, J. R., 2008. The Paleozoic Metamorphic History of the Central Orogenic Belt of China from $^{40}\text{Ar}/^{39}\text{Ar}$ Geochronology of Eclogite Garnet Fluid Inclusions. *Earth and Planetary Science Letters*, 268(3/4): 501–514. <https://doi.org/10.1016/j.epsl.2008.01.042>
- Renne, P. R., Swisher, C. C., Deino, A. L., et al., 1998. Intercalibration of Standards, Absolute Ages and Uncertainties in $^{40}\text{Ar}/^{39}\text{Ar}$ Dating. *Chemical Geology*, 145(1/2): 117–152. [https://doi.org/10.1016/S0009-2541\(97\)00159-9](https://doi.org/10.1016/S0009-2541(97)00159-9)
- Schneider, B., Kuiper, K., Postma, O., et al., 2009. $^{40}\text{Ar}/^{39}\text{Ar}$ Geochronology Using a Quadrupole Mass Spectrometer. *Quaternary Geochronology*, 4(6): 508–516. <https://doi.org/10.1016/j.quageo.2009.08.003>
- Smye, A. J., Warren, C. J., Bickle, M. J., 2013. The Signature of Devolatilisation: Extraneous ^{40}Ar Systematics in High-Pressure Metamorphic Rocks. *Geochimica et Cosmochimica Acta*, 113: 94–112. <https://doi.org/10.1016/j.gca.2013.03.018>
- Song, S. G., Zhang, L. F., Niu, Y. L., et al., 2005. Evolution from Oceanic Subduction to Continental Collision: A Case Study from the Northern Tibetan Plateau Based on Geochemical and Geochronological Data. *Journal of Petrology*, 47(3): 435–455. <https://doi.org/10.1093/ptrology/egi080>
- Song, S. G., Niu, Y. L., Su, L., et al., 2014. Continental Orogenesis from Ocean Subduction, Continent Collision/subduction, to Orogen Collapse, and Orogen Recycling: The Example of the North Qaidam UHPM Belt, NW China. *Earth-Science Reviews*, 129: 59–84. <https://doi.org/10.13039/501100001809>
- Turner, G., Wang, S. S., 1992. Excess Argon, Crustal Fluids and Apparent Isochrons from Crushing K-Feldspar. *Earth and Planetary Science Letters*, 110(1/2/3/4): 193–211. [https://doi.org/10.1016/0012-821x\(92\)90048-z](https://doi.org/10.1016/0012-821x(92)90048-z)
- Uunk, B., Postma, O., Wijbrans, J., et al., 2017. Direct $^{40}\text{Ar}/^{39}\text{Ar}$ Age Determination of Fluid Inclusions Using *in-vacuo* Stepwise Crushing—Example of Garnet from the Cycladic Blueschist Unit on Syros. 19th EGU General Assembly. 15117
- Villa, I. M., 2001. Radiogenic Isotopes in Fluid Inclusions. *Lithos*, 55(1/2/3/4): 115–124. [https://doi.org/10.1016/s0024-4937\(00\)00041-4](https://doi.org/10.1016/s0024-4937(00)00041-4)
- Wartho, J. A., Rex, D. C., Guise, P. G., 1996. Excess Argon in Amphiboles Linked to Greenschist Facies Alteration in the Kamila Amphibolite Belt, Kohistan Island Arc System, Northern Pakistan: Insights from $^{40}\text{Ar}/^{39}\text{Ar}$ Step-Heating and Acid Leaching Experiments. *Geological Magazine*, 133(5): 595–609. <https://doi.org/10.1017/s0016756800007871>
- Wijbrans, J. R., Pringle, M. S., Koppers, A. A. P., et al., 1995. Argon Geochronology of Small Samples Using the Vulkan Argon Laserprobe. *Proceedings Koninklijke Nederlandse Akademie van Wetenschappen*, 98(2): 185–218
- Yang, J. S., Xu, Z. Q., Song, S. G., et al., 2001. Discovery of Coesite in the North Qaidam Early Palaeozoic Ultrahigh Pressure (UHP) Metamorphic Belt, NW China. *Comptes Rendus de l'Académie des Sciences-Series IIA-Earth and Planetary Science*, 333(11): 719–724. [https://doi.org/10.1016/s1251-8050\(01\)01718-9](https://doi.org/10.1016/s1251-8050(01)01718-9)
- Zeitler, P. K., Fitz Gerald, J. D., 1986. Saddle-Shaped Age Spectra from Young, Microstructurally Complex Potassium Feldspars. *Geochimica et Cosmochimica Acta*, 50(6): 1185–1199. [https://doi.org/10.1016/0016-7037\(86\)90401-1](https://doi.org/10.1016/0016-7037(86)90401-1)
- Zhang, G. B., Zhang, L. F., Christy, A. G., 2013. From Oceanic Subduction to Continental Collision: An Overview of HP-UHP Metamorphic Rocks in the North Qaidam UHP Belt, NW China. *Journal of Asian Earth Sciences*, 63: 98–111. <https://doi.org/10.1016/j.jseas.2012.07.014>
- Zhang, G. B., Ellis, D. J., Christy, A. G., et al., 2009. UHP Metamorphic Evolution of Coesite-Bearing Eclogite from the Yuka Terrane, North Qaidam UHPM Belt, NW China. *European Journal of Mineralogy*, 21(6): 1287–1300. <https://doi.org/10.1127/0935-1221/2009/0021-1989>
- Zhang, J. X., Yang, J. S., Mattinson, C. G., et al., 2005. Two Contrasting Eclogite Cooling Histories, North Qaidam HP/UHP Terrane, Western China: Petrological and Isotopic Constraints. *Lithos*, 84(1/2): 51–76. <https://doi.org/10.1016/j.lithos.2005.02.002>
- Zheng, Y. F., Fu, B., Gong, B., et al., 2003. Stable Isotope Geochemistry of Ultrahigh Pressure Metamorphic Rocks from the Dabie–Sulu Orogen in China: Implications for Geodynamics and Fluid Regime. *Earth-Science Reviews*, 62(1/2): 105–161. [https://doi.org/10.1016/s0012-8252\(02\)00133-2](https://doi.org/10.1016/s0012-8252(02)00133-2)
- Zheng, Y. F., 2004. Fluid Activity during Exhumation of Deep-Subducted Continental Plate. *Chinese Science Bulletin*, 49(10): 985–998. <https://doi.org/10.1007/bf03184025>
- Zong, K. Q., Liu, Y. S., Hu, Z. C., et al., 2010. Melting-Induced Fluid Flow during Exhumation of Gneisses of the Sulu Ultrahigh-Pressure Terrane. *Lithos*, 120(3/4): 490–510. <https://doi.org/10.1016/j.lithos.2010.09.013>